Epithelial Rests of Malassez Form a Wnt-Dependent Mechanoresponsive Network

Peer-reviewed author version

Liu, B.; LAMBRICHTS, Ivo; Chang, E.; Torabi, M.M.; Aellos, F.; Ochweri, P.C.; Evens, I.; James, M.R.; Hakeam, M.A.; Huang, C.; Brunski, J.B.; HERMANS, Florian & Helms, J.A. (2026) Epithelial Rests of Malassez Form a Wnt-Dependent Mechanoresponsive Network. In: Journal of Dental Research,.

DOI: 10.1177/00220345261455868
Handle: http://hdl.handle.net/1942/49615

Epithelial rests of Malassez form a Wnt-dependent mechanoresponsive network

Bo Liu[1], Ivo Lambrichts[2], Elizabeth Chang[1], Mohammad Mahdi Torabi[1], Fabiana Aellos[1], Princess Cierra Ochweri[1], Inya Evens[2], Michael R. James[1,3], Mirna Abdal Hakeam[1], Caren Huang[1], John B. Brunski[1], Florian Hermans[2]*, and Jill A. Helms[1]*

1) Department of Surgery, Stanford University School of Medicine, Stanford CA 94304 USA

2) Department of Cardiology and Organ Systems (COS), Biomedical Research Institute (BIOMED), Faculty of Medicine and Life Sciences, Hasselt University, Diepenbeek, Belgium

3) Department of Biomedical Data Science, Stanford University, Stanford CA 94304 USA

* To whom correspondences should be addressed at florian.hermans@uhasselt.be and jhelms@stanford.edu

Short title: ERMs are mechanoresponsive network

Abstract word count: 290

Total word count: 3124

Figures: 4 plus 5 Appendix figures and 5 Appendix tables

References: 33

Abstract

Epithelial rests of Malassez (ERMs) constitute a three-dimensional epithelial meshwork extending from the tooth apex to the junctional epithelium (JE). This position, coupled observations from a variety of injury models, suggest that ERMs may be involved in sensing disruptions to the mechanical integrity of the periodontium. To test this hypothesis, finite element modeling was employed to predict strains states in tissues surrounding ERMs e.g., the periodontal ligament (PDL), supracrestal connective tissues, and the JE which, by virtue of their attachments to the tooth surface, experience distortional strains in response to mastication. An *in vivo* hyper-loading mouse model was employed to map these distortional strains to location-specific and time-dependent morphological changes in ERMs. Quantitative immunohistochemistry was used to interrogate ERMs for changes in expression of Piezo1, β4 integrin, Plectin, YAP, TRPV4, and phosphorylated FAK. Collagen and oxytalan fiber organization around ERMs was compared between conditions of normal- and hyper-loading. *Axin2Cre^{ERT2};R26R$^{mTmG/+}$* mice were used to lineage-trace Wnt-responsive ERMs under conditions of normal- and hyper-loading, and Wnt signaling from ERMs and the JE was disrupted using *K14Cre^{ERT2};Wls$^{fl/fl}$* mice.

Collectively, these analyses predicted that hyper-loading produced high distortional strains in the JE and supracrestal connective tissues, which correlated with sites of ERM enlargement. ERMs expressed mechanosensory proteins, whose levels were significantly elevated by hyper-loading. Load-activated ERMs were Wnt-responsive and if Wnt secretion was blocked then ERMs no longer expressed mechanosensory proteins and no longer enlarged in response to hyper-loading. A deterioration in the JE attachment and the PDL followed. Thus, the ERM network is positioned to sense distortional strains produced by mastication; they possess the molecular machinery to sense and respond to masticatory forces; and via a Wnt-dependent mechanism, coordinate tissue-level responses to mechanical loading in the PDL, supracrestal connective tissues and the JE.

Keywords

Mechanosensitive, mechanoresponsive, junctional epithelium, periodontal ligament, mechanical loading, PIEZO1

Introduction

The periodontium remodels in response to physical forces (Hine 1962). In the jaw skeleton, masticatory forces are transferred to the periodontium via the dentition and basic mechanics dictate that this

masticatory load is balanced by a set of equal and opposite loads that take the form of stresses and strains. When stresses and strains are excessive, they cause tissue damage (Shoham and Gefen 2012); when they are insufficient, the result is tissue atrophy (Pena et al. 2007). Between these extremes, stresses and strains stimulate remodeling of bone, the periodontal ligament (PDL), and the junctional epithelium (JE).

The dynamic nature of these mechanoadaptative responses is essential for maintaining overall health of the entire periodontium but how cellular responses are coordinated between the periodontal soft tissues remains an enigma. The JE, the supracrestal fibers, and the PDL are all bound to the tooth and thus experience stresses and strains in response to mastication (Jang et al. 2015; Yuan et al. 2023) but their distinct anatomical locations make it challenging to envision how their cellular responses are synchronized.

We considered one possibility, that these soft tissues possess a 'just in time' mechanism for dynamically adjusting to the amount of stress/strain applied. A feature of a just in time mechanism is that the system exists at a relatively low/inactive state until triggered e.g., in this case, by increased masticatory loading. In response to high distortional strains produced by hyper-loading, the system could then theoretically switch to an activated state and elicit a highly specific and localized molecular/cellular response, at the location of the increased load. This response to the amount of stress/strain would last only as long as needed to compensate for the increased demand. This kind of 'just in time' method, if it existed, would provide versatility in terms of cellular dynamics but would also depend on a mechanosensitive assembly (Eckert et al. 2025). Such a mechanosensitive assembly has not been described linking the JE, the supracrestal connective tissue, or PDL, but we hypothesized that the Epithelial Rests of Malassez (ERM) network could serve such a role.

Since their discovery by Serres (in 1817) and Malassez (Malassez 1885), there has been a deep interest in the origin, distribution and possible functions of ERMs (Keinan and Cohen 2013; Wesselink and Beertsen 1993; Xiong et al. 2013). ERMs appear in thin tissue sections as isolated islands of epithelial cells; in reality the tissue is a three-dimensional, fenestrated, mesh-like structure (Spouge 1984). This network, along with its extension from the root tip to immediately adjacent to the JE (Grant and Bernick 1969), struck us as ideally suited to sense strains within the tissues and potentially coordinate their responses to changes in mechanical input. The following *in silico*, *in vitro*, and *in vivo* experiments were undertaken to test this hypothesis.

Methods and materials

All experimental procedures followed ARRIVE 2.0 guidelines. Please see Appendix for animal husbandry and care, *in vivo* hyper- and hypo-loading models, collection, handling, and histological analyses of murine and

human tissues, single cell RNA-sequencing, quantitative immunohistochemistry (qIHC), and finite element (FE) modeling.

Results

Mastication produces distortional strains in the PDL and in the supracrestal region, which are elevated by hyper-loading.

FE modeling was to calculate the magnitude of distortional strains in the PDL, the supracrestal region, and JE under conditions of normal masticatory function, and under conditions of hyper-loading (Xu et al. 2019). The FE model was derived from µCT data (see Appendix, Methods) and material properties were assigned to soft and hard tissues as per (Fill et al. 2012; Nishihira 2003). Under conditions of normal masticatory load, the PDL experienced a mean distortional strain of 0.55% (+/- 0.45%; Fig. 1A). Under hyper-loading conditions the mean distortional strain in the PDL doubled, to 1.3% (+/- 0.45%; Fig. 1B,C).

By virtue of its hemidesmosomal attachment to the tooth, the JE also experiences distortional strains in response to normal masticatory forces (Yuan et al. 2023). The FE model predicted distortional strains in the JE/supracrestal region that were twice the magnitude experienced by the PDL (Fig. 1D,D',D" and F). Hyper-loading led to a mean level of JE distortional strain of 4.6 +/- 3.0% (Fig. 1E,E',E"), quadruple that experienced by the hyper-loaded PDL (Fig. 1F). When examined in detail, the highest strain centered on the supracrestal connective tissues (Fig. 1E',E").

ERMs in the supracrestal region are larger than ERMS along the root

The PDL and JE are anatomically distinct structures but based on their shared attachments to a moving tooth, their responses to hyper-loading would likely be coordinated to provide appropriate tissue level responses. We hypothesized that the 3D ERM meshwork was a candidate tissue for this task. ERMs were observed in the PDL space (Fig. 1G,H) and the supracrestal connective tissue, coronal to the alveolar bone crest (Fig. 1G,I), under normal masticatory loading conditions. The size of these anatomically distinct ERMs was quantified (see Methods) and those in the supracrestal region were consistently, significantly larger than those along the root (green bars, Fig. 1J).

Hyper-loading triggers the selective expansion of supracrestal ERMs

Larger ERMs were located in the supracrestal region, which experienced higher distortional strains compared to the PDL space (Fig. 1). To test whether the size or number of ERMs was influenced by strain, an *in vivo* hyper-loading model was employed (see Methods and (Xu et al. 2019)). The periodontium of teeth subjected to hyper-loading for 3, 7, 14, and 28 days was compared against baseline data from periodontia subjected to normal masticatory loading (Fig. 1J).

Within 1 day of hyper-loading, more ERMs were detected (yellow arrows, Fig. 1K; quantified in L). The total number of ERMs increased between days 1 and 3, and again between days 3 and 7 of hyper-loading (Fig. 1L). After 7 days of hyper-loading the number of ERMs remained relatively constant, and always significantly more than observed around normal loading controls (Fig. 1L).

Changes in ERM size were also observed. Under hyper-loading conditions, supracrestal ERMs were larger than root ERMs (compare Fig. 1M,N) and over the duration of hyper-loading this difference in size became more pronounced (Fig. 1O). Thus, ERM number and size exhibited a time-dependent responsiveness to masticatory hyper-loading.

Hyper-loading by itself does not trigger periodontal inflammation

Factors other than mechanical force could influence ERM number and/or size. For example, hyper-loading could cause an inflammatory response (Leone et al. 2026), which indirectly affected the number and size of ERMs. To evaluate this possibility, the distribution and number of neutrophils and macrophages in the hyper-loading group was compared to controls subjected to normal masticatory loading. No apparent differences between hyper-loaded and control groups in terms of neutrophil and macrophage number and distribution in either the PDL space, or the JE were observed (Appendix Fig. 1).

Supracrestal ERMs expand in response to hyper-loading

Hyper-loading correlated with an increase in the number and size of ERMs; we next tested whether hypo-loading had the opposite effect. After 4 weeks of hypo-loading (see Methods and (Zhang et al. 2019)), ERMs along the root surface (Fig. 1P,Q) and ERMs in the supracrestal region (Fig. 1P,R) were significantly smaller compared to both controls and the hyper-loaded group (Fig. 1S). These data further supported the conclusion that the ERM network was responsive to changes in masticatory forces.

ERMs are mechanoresponsive

Do ERMs possess the molecular machinery to detect a physical force and convert it into a biochemical signal? Human ERMs expressed the mechanically gated ion channel Piezo1 (Fig. 2A); single cell RNA-sequencing (scRNA-seq) data confirmed expression of Piezo1 in human ERMs and in JEs (Fig. 2B). The mechanosensitive adhesion protein β4 integrin (Fig. 2C,D), the mechanosensitive linker protein Plectin (Fig. 2E,F), and the mechanoresponsive ion channel TRPV4 (Fig. 2G,H) were also detected in human ERMs and in the JE.

Murine ERMs also expressed Piezo1 (Fig. 2I), and its expression was significantly elevated in load-activated ERMs (Fig. 2J,K). The mechanosensitive proteins β4 integrin (Fig. 2L,M) and Plectin (Fig. 2N,O), as well as

TRPV4 (Fig. 2P,Q) and YAP (Fig. 2R,S), were all expressed in ERMs under both normal and hyper-loading conditions, with expression being consistently higher in ERMs induced by hyper-loading.

Of particular note was the pattern of phosphorylated focal adhesion kinase (phosphor-FAK) expression in ERMs under normal and hyper-loading conditions (Fig. 2T,U). Phalloidin staining identified F-actin+ microfilaments (Fig. 2V), and co-localization with phospho-FAK (Fig. 2V,W,X) provided strong evidence that ERMs were involved in transducing mechanical signals into biochemical signals.

ERMs initiate matrix remodeling in response to hyper-loading

Thus far, our data demonstrated that ERMs possess the molecular machinery to sense and respond to mechanical forces; we postulated these forces were transmitted to ERMs via surrounding connective tissue fibers. Transmission electron microcopy illustrated the proximity of human ERMs to collagen fibers (Fig. 3A) and to oxytalan fibers (Fig. 3B). Histological staining for oxytalan fibers illustrated their close association with ERMs (Fig. 3C). βIII tubulin+ neurons encircled ERMs (red arrow, Fig. 3D). Expression of matrix metalloproteinase 13 (MMP13) in ERMs suggested their local extracellular matrix was prone to remodeling.

Similar relationships were noted between murine ERMs and picrosirius red-stained collagen fibers (Fig. 3F), and purple-stained oxytalan fibers, which are typically oriented perpendicular to collagen fibers (Fig. 3G,H). βIII tubulin+ neurons were in close proximity to murine ERMs (red arrow, Fig. 3I). Murine ERMs were also immunopositive for MMP13 (Fig. 3J).

Hyper-loading in the mouse model resulted in apparent collagen fiber micro-ruptures (Fig. 3K, Appendix Fig. 2); collagen content analyses indicated that continued hyper-loading was detrimental to fiber density (Fig. 3L). Fragmented oxytalan fibers were also evident around load-activated ERMs (Fig. 3M, Appendix Fig. 2). Load-induced damage to the extracellular matrix correlated with significantly increased expression of MMP13 in and around murine ERMs (Fig. 3N,O).

ERMs release Wnt signals that influence the mechanoresponsiveness of the PDL

To coordinate mechanosensitive responses in the PDL, supracrestal connective tissue, and JE we speculated that load-activated ERMs released signaling molecules that could locally influence cellular behavior. The following lines of evidence implicated Wnt/β-catenin signaling in this process.

The first line of evidence came from lineage-tracing the fates of Wnt-responsive cells in ERMs. Tamoxifen was delivered to the Wnt lineage tracer strain *Axin2Cre^{ERT2};R26R$^{mTmG/+}$*. Three days later, small, Keratin5+ ERMs, some of which co-stained with GFP, were detected (Fig. 4A-A"). Very few PCNA+ cells were detectable

in the PDL (Appendix Fig. 3), indicating that under normal loading conditions, Wnt-responsive ERMs were generally quiescent.

The second line of evidence came from fate-mapping Wnt responsive cells under conditions of hyper-loading. Tamoxifen was delivered to *Axin2Cre^{ERT2};R26R$^{mTmG/+}$* mice and immediately thereafter hyper-loading was initiated. After 3 days, Keratin5+ ERMs were significantly larger (arrows, Fig. 4B; quantified in Fig. 1) and the number of Wnt-responsive cells increased (Fig. 4B',B"), which corresponded with an increase in PCNA+ cells in the PDL (Appendix Fig. 3). The majority of Wnt-responsive cells were positioned adjacent to the cementum, and some co-localized with the Keratin5+ ERMs (Fig. 4B-B").

After 7 days of hyper-loading the number and size of ERMs continued to significantly increase (arrows, Fig. 4C-C"; quantified in Fig. 1); load-activated ERMs maintained their Wnt-responsive status (Fig. 4C-C"). GFP+ Wnt-responsive cells remained associated with the enlarged Keratin5+ ERMs throughout longer periods of hyper-loading (Fig. 4D-D"). Together, these data strongly suggested that Wnt signaling was involved in ERM responses to hyper-loading.

To directly test whether Wnt signals emanated from ERMs, a K14Cre driver was crossed with a *Wntless$^{fl/fl}$* strain. GFP immunostaining in *K14Cre^{ERT2};R26R$^{mTmG/+}$* mice confirmed tissue specificity of the Cre to ERMs (Appendix Fig. 4) and the JE, then *K14Cre^{ERT2};Wls$^{fl/fl}$* mice were generated. The chaperone protein Wntless (Wls) is essential for Wnt protein secretion (Banziger et al. 2006), and immunostaining for nuclear β-catenin confirmed that canonical Wnt signaling was inhibited in ERMs of *K14Cre^{ERT2};Wls$^{fl/fl}$* mice (compare Fig. 4E,F).

A third line of evidence that Wnt/β-catenin was involved in ERM signaling came from molecular analyses. Seven days after tamoxifen delivery, expression of Piezo1 (Fig. 4G-I) and YAP (Fig. 4J-L) were lost in *Wls* mutant ERMs. β4 integrin expression was absent in *Wls* mutant ERMs, and in *Wls* mutant JEs (compare Fig. 4M,N; quantified in O; P,Q; quantified in R). These data demonstrated that Wnt/β-catenin signaling was required for ERM mechanosensitivity, as well as JE attachment.

Our fourth line of evidence supporting an essential role for Wnt/β-catenin signaling in ERM mechanotransduction came from analyses of *Wls* mutant mice after initiating hyper-loading. Normally, supracrestal ERMs enlarge in response to hyper-loading; in *Wls* mutants these supracrestal ERMs did not expand (compare Fig. 4S,T; quantified in U). In addition to defects in the JE and supracrestal region, PDL fibers deteriorated. Picrosirius red-stained collagen fibers in the PDL of control mice exhibited their characteristically dense, linear, elongated morphology (Fig. 4V). In *Wls* mutants, PDL fibers were sparse, fragmented and truncated (Fig. 4W).

Discussion

Functionless relics- or an essential mechanosensory element in the periodontium?

The vestige of (Hertwig's) epithelial root sheath, ERMs emerge during tooth development and endure for the lifetime of most mammals (Reitan 1961). Embryonic tissues are equipped to remove redundant cells (Abud 2004); consequently, this persistence of an ERM network argues against them being simply "developmental jetsam" (Cohen 1976). We started this study by asking, why does this ERM network persist? And what are the circumstances that provoke ERM reactivation?

The ERM network is ideally positioned to detect and respond to mechanical input

Our hypothesis was that ERMs function as a mechanotransducing network, which is supported by four lines of evidence. First, ERMs are embedded in a mechanoresponsive extracellular matrix (ECM). ERMs in supracrestal connective tissues are encircled by collagen and oxytalan fibers, and because the JE and supracrestal fibers are firmly attached to the tooth surface, these tissues along with supracrestal ERMs experience stresses and strains created by masticatory loading (Fig. 1). The same relationship holds true in the PDL space: because of its attachment to the tooth surface, the PDL and root ERMs experience stresses and strains in response to masticatory forces (Fig. 1). Thus, the ERM network appears to be ideally positioned to detect and respond to changes in mechanical loading of the dentition.

ERMs are responsive to changes in masticatory load

Hyper-loading of the dentition triggers an increase in the size and number of ERMs; conversely, hypo-loading results in a significant reduction in ERM size (Fig. 1). This change in size is most significant in the supracrestal region, where distortional strains are twice as high as in the PDL (Fig. 1). These experiments demonstrate a correlation between mechanical loading and ERM biology.

Hyper-loading is not the sole stimulus that leads to ERM activation. ERM "reactivity", especially in the supracrestal region, has been observed after severing supracrestal fibers in a gingivectomy procedure (Ramfjord et al. 1966), after orthodontic tooth movement (Gilhuus-Moe and Kvam 1972; Talic et al. 2003), after ligature-induced periodontitis (Manisagian et al. 2018), and in a variety of genetic models of periodontal disease (Sojod et al. 2017; Wang et al. 2018). A shared feature of all these conditions is that they disrupt the mechanical integrity of the periodontium. Thus, our proposed function for the ERM as a mechanosensory network aligns with ERM activation in these other models of injury and/or disease.

ERMs possess the molecular machinery for mechanotransduction

The third line of evidence supporting our hypothesis that ERMs function as a mechanotransducing network is the fact that ERMs express multiple proteins with well-described mechanosensitive and

mechanoresponsive functions (Fig. 2). ERM-specific expression of mechano-sensitive and -responsive proteins significantly increases in response to hyper-loading (Fig. 2). The fact that hyper-loading led to increased expression of the mechanosensory proteins further suggests that ERMs adjust this molecular machinery to adapt to a changing mechanical environment, perhaps via a positive feedback loop. Other epithelial tissues harbor such a positive feedback loop involving Piezo1 and Wnt/β-catenin signaling (He et al. 2024).

ERMs function as an essential Wnt-dependent mechanotransducive network

Several studies confirm that Wnt signaling is directly regulated by mechanical cues (Li et al. 2021; Oak et al. 2025; Przybyla et al. 2016; Zhou et al. 2020) and our fourth line of evidence supporting a mechanoresponsive function for ERMs came from studies involving manipulation of Wnt/β-catenin signaling in ERMs. fate-mapping experiments demonstrated that ERMs and significantly, load-induced ERMs, are Wnt-responsive (Fig. 4).

The essential role for Wnt signaling in ERM mechanotransduction was demonstrated by genetically deleting the *Wls* from K14-expressing cells. This strategy resulted in loss of mechanosensitive protein expression in ERMs (Fig. 4). ERMs typically expand in response to hyper-loading (Fig. 1) but Wnt-deficient supracrestal ERMs failed to enlarge, demonstrating that they were no longer sensitive to mechanical input (Fig. 4). In the *Wls* mutant, PDL fibers were thin, short, and sparse and the JE began to lose its attachment (Fig. 4). Together these data support our conclusion that the ERM network functions as a Wnt-dependent mechanosensor.

Limitations of the current study

In this study we integrated analyses conducted in human tissues with analyses of murine tissues, and one might legitimately ask whether tissues from two species should be compared. There are multiple variables to consider: for example, It was not possible to ascertain if patients from which ERMs were collected had normal masticatory function or not whereas a mouse model permitted control over variables such as masticatory loading. There is also the issue of age: in humans, ERM numbers change with age (Simpson 1965) and in our study, murine age was kept constant. Consequently, we are comparing not only different species, but tissues from different life stages. Further, human samples come from a genetically diverse population whereas our murine population is far more genetically homogeneous.

Despite these and other differences, there are two major justifications for undertaking such comparisons. First, in both species, ERMs share a developmental origin e.g., the ERS. This shared origin suggests a conserved biological identity and, potentially, conserved functions. Second, the signaling pathways controlling tooth development and periodontal homeostasis e.g., Wnt, Notch, Shh, BMP are highly

conserved across mammals; consequently, it is reasonable to presume that the mechanisms controlling ERM quiescence/activation are substantially the same in both species. Finally, human tissues allow us to make observations about ERMs, from which we can make hypotheses that are testable within a mouse model. If our experimental data support a particular hypothesis, we may then be able to formulate therapeutic strategies based on those animal models that have potential value in treating human disease.

Conclusions

ERMs are positioned in the right place and at the right time to sense distortional strains produced by masticatory loading. ERMs possess the molecular machinery to sense and respond to masticatory loading and alter their size and number in response to hyper-loading. ERMs use a Wnt-dependent mechanism to coordinate tissue-level responses to physical forces delivered by mastication. Together these data support the conclusion that the ERM meshwork functions as a mechanosensory organ and is a critical part of how periodontal tissues cope with functional changes in their mechanical environment.

Author contributions

Bo Liu and Florian Hermans contributed to the conception and design of the study, data acquisition, analysis, and interpretation, as well as drafting and critically revising the manuscript. Elizabeth Chang, Mohammad Mahdi Torabi, Fabiana Aellos, Princess Cierra Ochweri, Inya Evens, Mirna Abdal Hakeam and Caren Huang contributed to data acquisition, analysis, and interpretation, and critically revised the manuscript. Michael Rutherford James contributed to statistical analyses and interpretation, and critically revised the manuscript. John Brunski formulated the finite element (FE) modeling of the relevant tissues and critically revised the manuscript. Ivo Lambrichts and Jill A. Helms contributed to the study's conception, design, analysis, and interpretation, as well as drafting and critically revising the manuscript. All authors provided final approval and agreed to be accountable for all aspects of the work.

Acknowledgements

We would like to acknowledge the anonymous reviewers selected by JDR to evaluate this work. Their expertise, along with their queries and criticisms, reflected deep knowledge and insight into the biology of ERMs. Their questions prompted us to undertake a number of additional experiments that ultimately improved this manuscript and for that, we are grateful.

F.H. was supported by the Fund for Scientific Research (FWO)- Flanders (Belgium) (1226325N to F.H.). I.L. and F.H. were supported by the FWO (G0A2E26N). B.L., M.M.T. and J.A.H. were supported by NIH 1R01DE031270-01A1 and NIH 1R25DE03355901A1 to J.A.H.

Computational resources for all single cell transcriptome analyses were provided by the 'Vlaams Supercomputer Centrum' (VSC), managed by the FWO. Computational resources for all single cell transcriptome analyses were provided by the 'Vlaams Supercomputer Centrum' (VSC), managed by the FWO.

Data Availability Statement

The data and materials that support the findings of this study are publicly available. Histological and immunohistochemical images are deposited in the Stanford Digital Repository (DOI: https://doi.org/10.25740/mk437kj0019). Gene expression analysis in human ERM was performed using publicly available human PDL data (GEO accession number GSE161266).

Competing interests

The authors declare no competing or financial interests.

Figure legends

Figure 1. ERMs respond to distortional strains in the PDL, the JE and the supracrestal connective tissues.

(A) Finite Element (FE) modeling of the PDL space, showing distribution of distortional strains under conditions of normal- and (B) hyper-loading. (C) Mean distortional strains in the PDL produced by normal- and hyper-loading. (D) FE model of the JE and supracrestal connective tissue, showing distribution of distortional strains under conditions of (D,D') normal- and (E,E') hyper-loading. (D",E") The highest distortional strains are concentrated in the basal JE and supracrestal region (arrows). (F) Mean distortional strains in the JE/supracrestal region produced by normal and hyper-loading. (G) Pentachrome histology of a tooth under normal loading; note ERMs in the root and supracrestal regions (arrows). (H) Higher magnification image, illustrating the average size of root ERMs (arrow) and (I) supracrestal ERMs (arrow) around a dentition subjected to normal loading. (J) Quantification of ERM size as a function of location under normal loading conditions. (K) Pentachrome histology of a tooth under hyper-loading; note multiple ERMs in the root and supracrestal regions (yellow arrows). (L) Quantification of ERM number as a function of the duration of hyper-loading. (M) Higher magnification image, illustrating root ERMs (arrows) and (N) supracrestal ERMs (arrows) around a dentition subjected to hyper-loading. (O) Quantification of ERM size as a function of location, loading regimen, and duration of the hyper-loading condition. (P) Pentachrome

histology of a tooth under hypo-loading; note ERMs in the root and supracrestal regions (arrows). (Q) Higher magnification image illustrating the average size of root ERMs (arrow) and (R) supracrestal ERMs (arrows) around a dentition subjected to hypo-loading. (S) Quantification of ERM size as a function of loading regimen. Abbreviations: ab, alveolar bone; JE, junctional epithelium. One asterisk indicates a p value ≤0.05; Two asterisks indicate a p value ≤0.01; Three asterisks indicate a p value ≤0.001; Four asterisks indicate a p value ≤0.0001.

Figure 2. ERMs express mechanosensitive and mechanoresponsive proteins.
Human ERMs express (A) PIEZO1, which was confirmed via (B) scRNA-seq analysis. Expression of PIEZO1 in ERMs (green) was compared to its expression in the JE (blue). (C) β4 INTEGRIN immunostaining in a representative human ERM; (D) scRNA-seq analysis confirmed expression in ERMs (green) and JE (blue). (E) PLECTIN immunostaining in a human ERM, confirmed by (F) scRNA-seq analysis. (G) Human ERMs express TRPV4, confirmed by (H) scRNA-seq analysis. Murine ERMs (arrows) express Piezo1 under (I) normal loading and (J) hyper-loading conditions; (K) quantification of Piezo1. Murine ERMs (arrows) also express (L,M) β4 integrin, (N,O) Plectin, (P,Q) TRVP4 , (R,S) YAP, and (T,U) phosphorylated FAK under normal and hyper-loading conditions. (V) Phalloidin staining identifies F-actin in an ERM that (W) co-localizes with phospho-FAK, indicating (X) that ERMs are actively responding to mechanical stimuli under conditions of mechano-loading. Abbreviations: c, cementum; d, dentin. Asterisks as indicated in Fig. 1.

Figure 3. Remodeling of the extracellular matrix around ERMs is stimulated by hyper-loading.
Representative transmission electron microscopic images showing (A) collagen fibers and (B) oxytalan fibers encircling ERMs. (C) Human ERMs stained with Oxytalan staining to illustrate circumferential oxytalan fibers. Immunostaining for (D) βIII tubulin; red arrow indicates a βIII tubulin+ neuron and (E) MMP13. Representative images from murine tissues (F) stained with picrosirius red and visualized under polarized light to visualize collagen fibers, and (G,H) stained with Gomori's aldehyde fuchsin to visualize oxytalan fibers. (I) Immunostaining for (I) βIII tubulin; red arrow indicates a βIII tubulin+ neuron and (J) MMP13. Under hyper-loading conditions, (K) collagen-stained fibers around ERMs appear fragmented. (L) Collagen density around ERMs as a function of the duration of hyper-loading. Under hyper-loading conditions, (M) oxytalan-stained fibers around ERMs appear truncated (N) MMP13 expression in ERMs is significantly increased under hyper-loading conditions. Abbreviations: c, cementum; d, dentin; col, collagen; oxy, oxytalan; je, junctional epithelium; PDL, periodontal ligament; erm, epithelial rests of Malassez. Asterisks: as indicated in Fig. 1.

Figure 4. Supracrestal ERMs adjacent to the JE show the most significant enlargement in response to hyper-loading.

Axin2Cre^{ERT2};R26R$^{mTmG/+}$ mice received tamoxifen and 3 days later immunostaining for (A) Keratin5 and (A') GFP identified (A") Wnt-responsive ERMs under normal loading conditions. *Axin2Cre^{ERT2};R26R$^{mTmG/+}$* mice under conditions of hyper-loading for 3 days, followed by immunostaining for (B) Keratin5 and (B') GFP to identify (B") Wnt-responsive ERMs. Under hyper-loading conditions for (C,C',C") 7 days and (D,D',D") 14 days. Seven days after tamoxifen delivery, comparison of β-catenin immunostaining in ERMs of (E) control and (F) *Wls* mutant mice. Expression of Piezo1 in in ERMs of (G) control and (H) *Wls* mutant mice; quantified in (I). Expression of YAP in in ERMs of (J) control and (K) *Wls* mutant mice; quantified in (L). Expression of β4 integrin ERMs of (M) control and (N) *Wls* mutant mice; quantified in (O); and in the JE of (P) control and (Q) *Wls* mutant mice; quantified in (R). Supracrestal ERMs size in (S) control and (T) *Wls* mutant mice; size quantified in (U). Picrosirius red-stained collagen in the PDL space of (V) control and (W) *Wls* mutant mice. Dotted white lines indicate root surfaces. Abbreviations: c, cementum; d, dentin. Asterisks as indicated in Fig. 1.

References

Abud HE. 2004. Shaping developing tissues by apoptosis. Cell Death Differ. 11(8):797-799.

Banziger C, Soldini D, Schutt C, Zipperlen P, Hausmann G, Basler K. 2006. Wntless, a conserved membrane protein dedicated to the secretion of wnt proteins from signaling cells. Cell. 125(3):509-522.

Cohen B. 1976. The enigma of vestigial tissues. Ann R Coll Surg Engl. 58(2):104-114.

Eckert J, Viasnoff V, Yap AS. 2025. New directions in epithelial mechanoadaptation. Curr Opin Cell Biol. 95:102536.

Fill TS, Toogood RW, Major PW, Carey JP. 2012. Analytically determined mechanical properties of, and models for the periodontal ligament: Critical review of literature. J Biomech. 45(1):9-16.

Gilhuus-Moe O, Kvam E. 1972. Behaviour of the epithelial remnants of malassez following experimental movement of rat molars. Acta Odontol Scand. 30(2):139-149.

Grant DA, Bernick S. 1969. A possible continuity between epithelial rests and epithelial attachment in miniature swine. J Periodontol. 40(2):87-95.

He J, Cheng X, Fang B, Shan S, Li Q. 2024. Mechanical stiffness promotes skin fibrosis via piezo1-wnt2/wnt11-ccl24 positive feedback loop. Cell Death Dis. 15(1):84.

Hine MK. 1962. Periodontal traumatism. J Dent Res. 41:290-299.

Jang AT, Merkle AP, Fahey KP, Gansky SA, Ho SP. 2015. Multiscale biomechanical responses of adapted bone-periodontal ligament-tooth fibrous joints. Bone. 81:196-207.

Keinan D, Cohen RE. 2013. The significance of epithelial rests of malassez in the periodontal ligament. Journal of endodontics. 39(5):582-587.

Leone P, Thomas JT, Sorsa T, Kononen M, Anil S. 2026. Occlusal overload and periodontitis: Integrating mechanisms, clinical evidence, and emerging perspectives-a scoping review. International journal of dentistry. 2026:9936924.

Li Y, Chen M, Hu J, Sheng R, Lin Q, He X, Guo M. 2021. Volumetric compression induces intracellular crowding to control intestinal organoid growth via wnt/beta-catenin signaling. Cell Stem Cell. 28(1):170-172.

Malassez L. 1885. Sur l'existence d'amas épithéliaux autour de la racine des dents chez l'homme adulte et a l'état normal. Arch de Physiol 3e(5):129.

Manisagian GEP, Benedí D, Goya JA, Mandalunis PM. 2018. Study of epithelial rests of malassez in an experimental periodontitis model. Acta Odontologica Latinoamericana: AOL. 31(3).

Nishihira MYKSYIHNAN. 2003. Dental biomechamics. Natali AN, editor. London: CRC Press.

Oak ASW, Bagchi A, Brukman MJ, Toth J, Ford J, Zheng Y, Nace A, Yang R, Hsieh JC, Hayden JE et al. 2025. Wnt signaling modulates mechanotransduction in the epidermis to drive hair follicle regeneration. Sci Adv. 11(8):eadq0638.

Pena E, Calvo B, Martinez MA, Doblare M. 2007. On finite-strain damage of viscoelastic-fibred materials. Application to soft biological tissues. International Journal for Numerical Methods in Engineering. 74(7).

Przybyla L, Lakins JN, Weaver VM. 2016. Tissue mechanics orchestrate wnt-dependent human embryonic stem cell differentiation. Cell Stem Cell. 19(4):462-475.

Ramfjord SP, Engler WO, Hiniker JJ. 1966. A radioautographic study of healing following simple gingivectomy. Ii. The connective tissue. J Periodontol. 37(3):179-189.

Reitan K. 1961. Behavior of malassez' epithelial rests during orthodontic tooth movement. Acta Odontol Scand. 19:443-468.

Shoham N, Gefen A. 2012. Deformations, mechanical strains and stresses across the different hierarchical scales in weight-bearing soft tissues. J Tissue Viability. 21(2):39-46.

Simpson HE. 1965. The degeneration of the rests of malassez with age as observed by the apoxestic technique. J Periodontol (1930). 36:288-291.

Sojod B, Chateau D, Mueller CG, Babajko S, Berdal A, Lezot F, Castaneda B. 2017. Rank/rankl/opg signalization implication in periodontitis: New evidence from a rank transgenic mouse model. Frontiers in physiology. 8:338.

Spouge JD. 1984. The rests of malassez and chronic marginal periodontitis. J Clin Periodontol. 11(5):340-347.

Talic NF, Evans CA, Daniel JC, Zaki AE. 2003. Proliferation of epithelial rests of malassez during experimental tooth movement. Am J Orthod Dentofacial Orthop. 123(5):527-533.

Wang Y, Liu M, Deng S, Sui X, Fan L, Zhang Q. 2018. Osteoprotegerin deficiency causes morphological and quantitative damage in epithelial rests of malassez. J Mol Histol. 49(3):329-338.

Wesselink PR, Beertsen W. 1993. The prevalence and distribution of rests of malassez in the mouse molar and their possible role in repair and maintenance of the periodontal ligament. Arch Oral Biol. 38(5):399-403.

Xiong J, Gronthos S, Bartold PM. 2013. Role of the epithelial cell rests of malassez in the development, maintenance and regeneration of periodontal ligament tissues. Periodontol 2000. 63(1):217-233.

Xu Q, Yuan X, Zhang X, Chen J, Shi Y, Brunski JB, Helms JA. 2019. Mechanoadaptive responses in the periodontium are coordinated by wnt. J Dent Res. 98(6):689-697.

Yuan X, Liu B, Cuevas P, Brunski J, Aellos F, Petersen J, Koehne T, Broer S, Gruber R, LeBlanc A et al. 2023. Linking the mechanics of chewing to biology of the junctional epithelium. J Dent Res. 102(11):1252-1260.

Zhang X, Yuan X, Xu Q, Arioka M, Van Brunt LA, Shi Y, Brunski J, Helms JA. 2019. Molecular basis for periodontal ligament adaptation to in vivo loading. J Dent Res. 98(3):331-338.

Zhou T, Gao B, Fan Y, Liu Y, Feng S, Cong Q, Zhang X, Zhou Y, Yadav PS, Lin J et al. 2020. Piezo1/2 mediate mechanotransduction essential for bone formation through concerted activation of nfat-yap1-ss-catenin. Elife. 9.

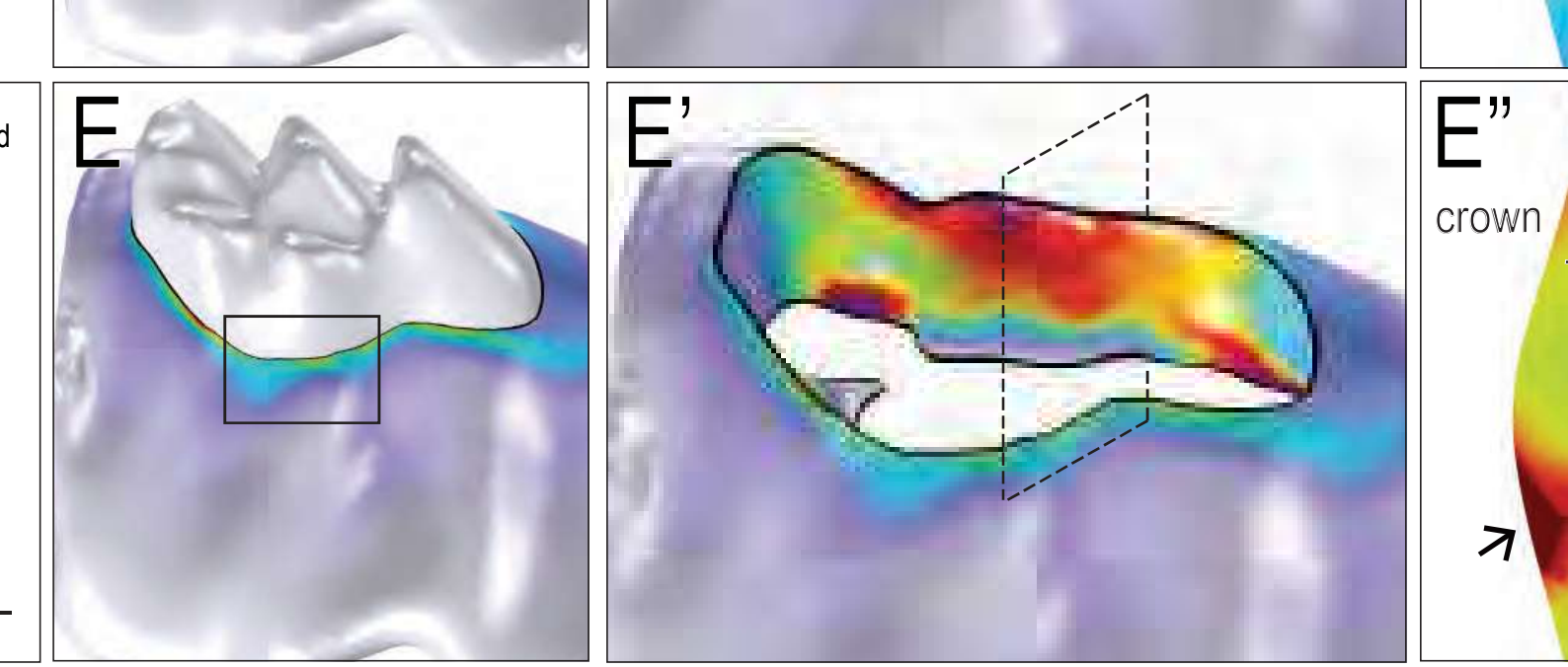

Root ERMs

Supracrestal ERMs

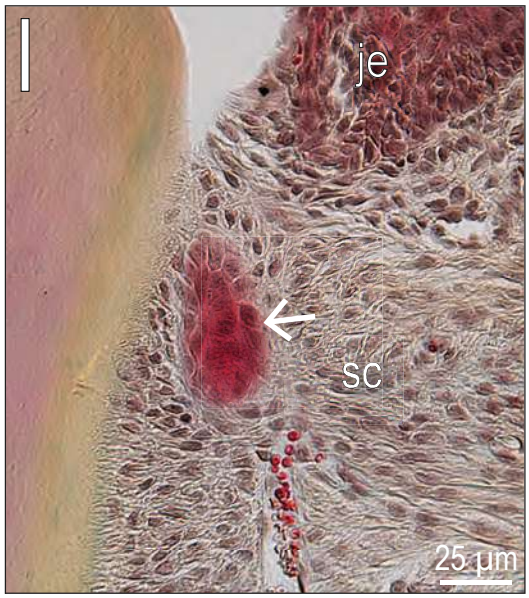

ERM size, by location

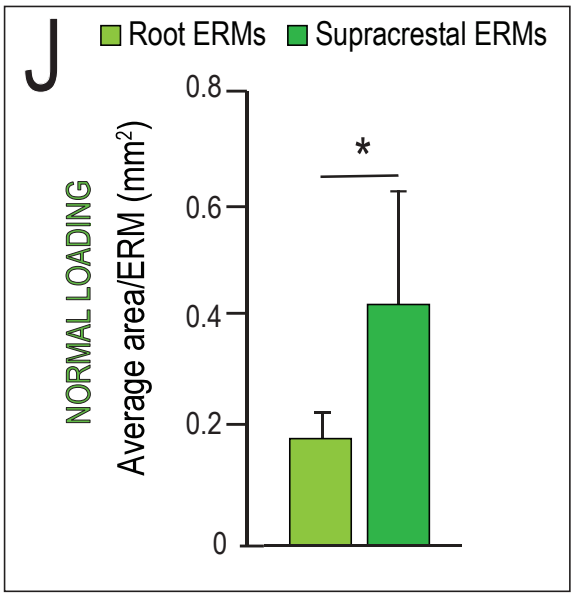

M number over time

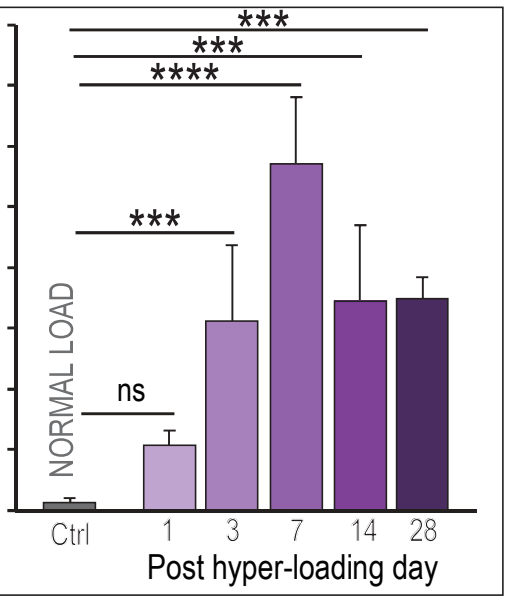

Root ERMs

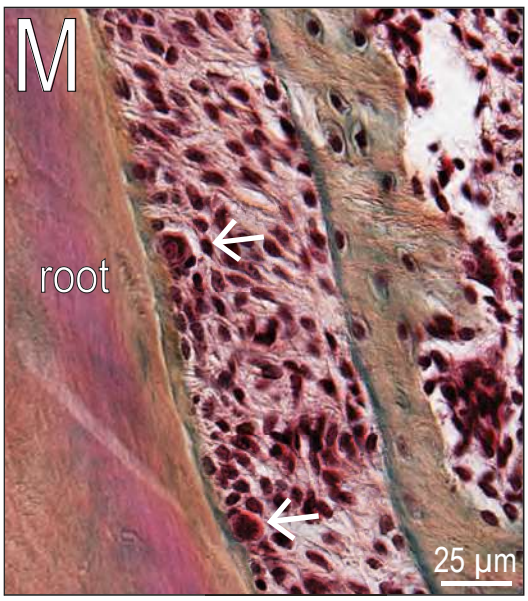

Supracrestal ERMs

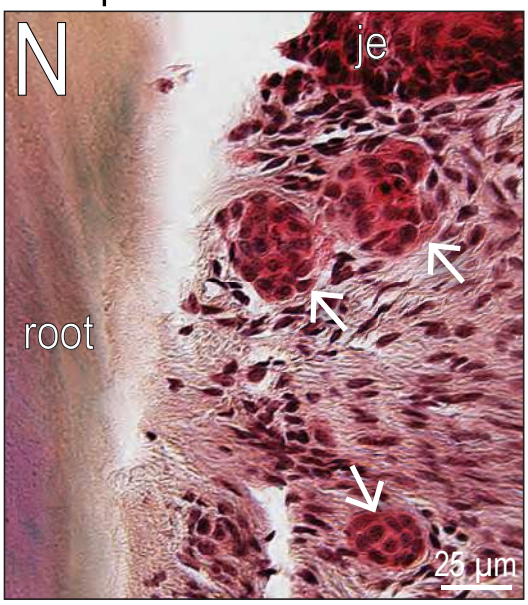

Root ERMs

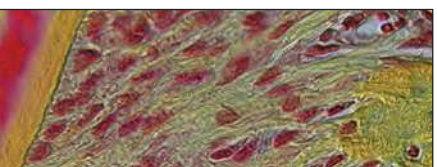

Supracrestal ERMs

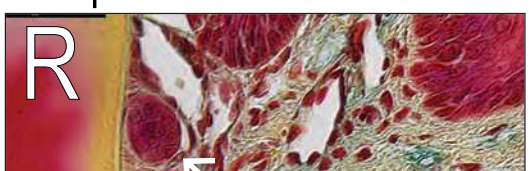

ERM size

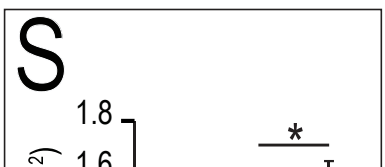

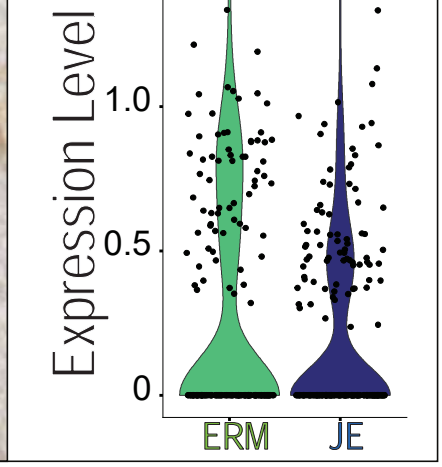

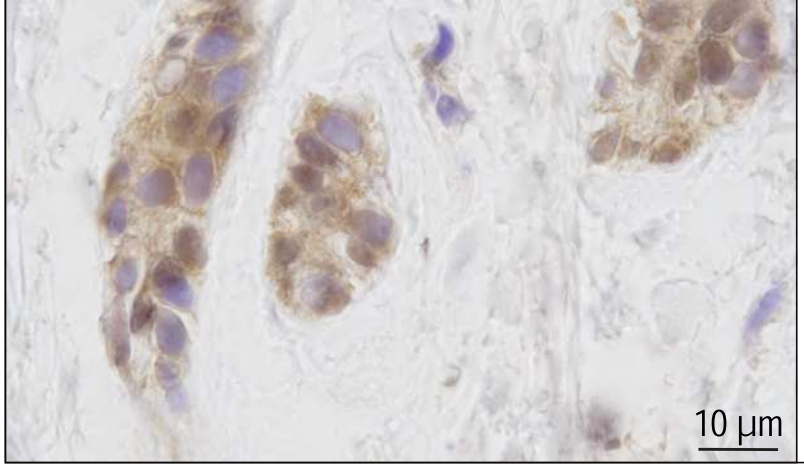

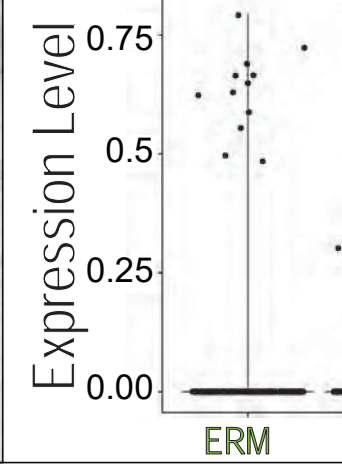

β4 integrin

Plectin

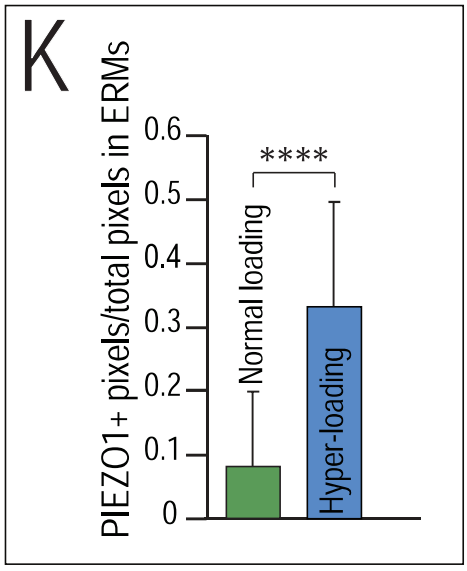

Normal loading

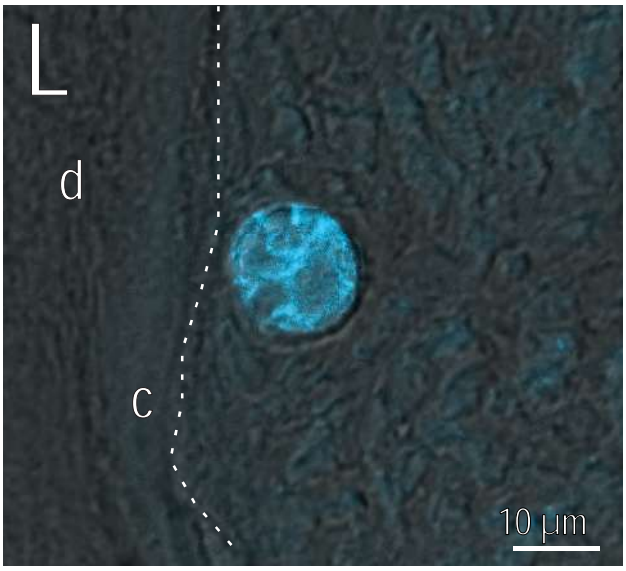

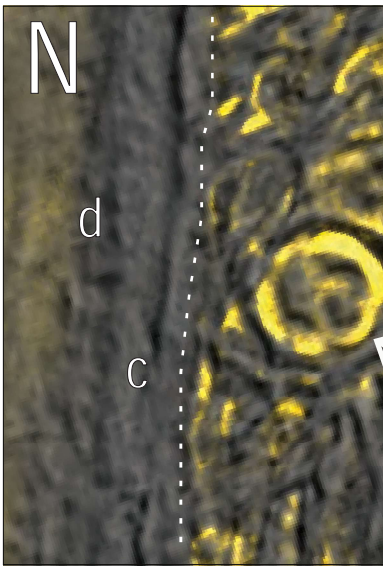

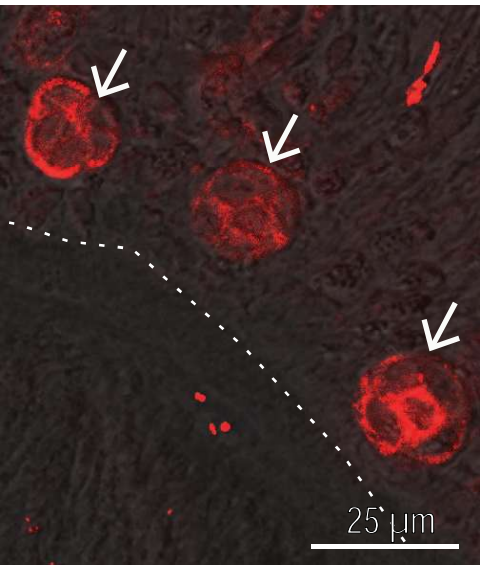

Hyper-loading

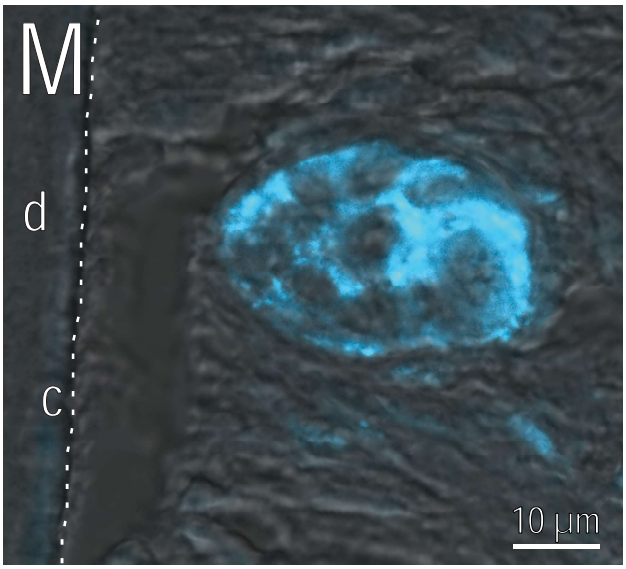

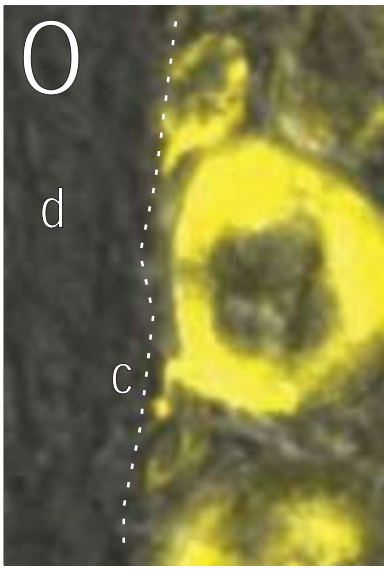

YAP/DAPI

phospho-FAK

Pha

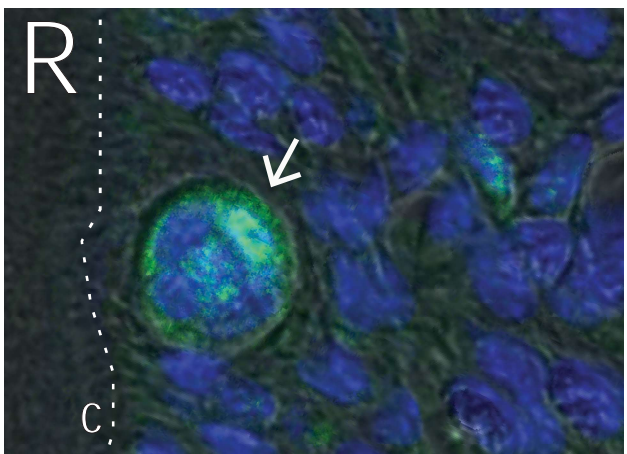

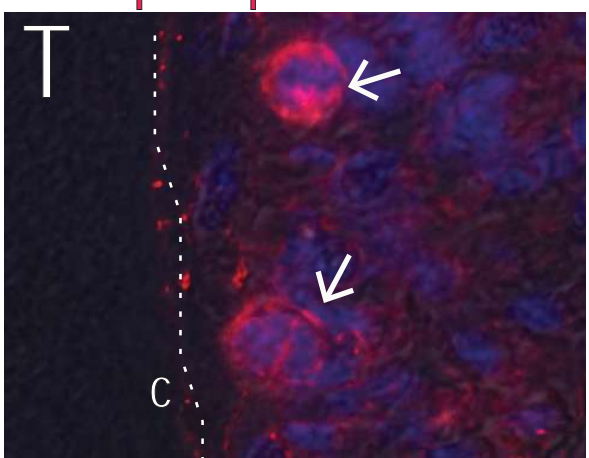

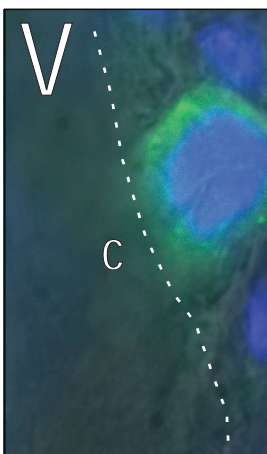

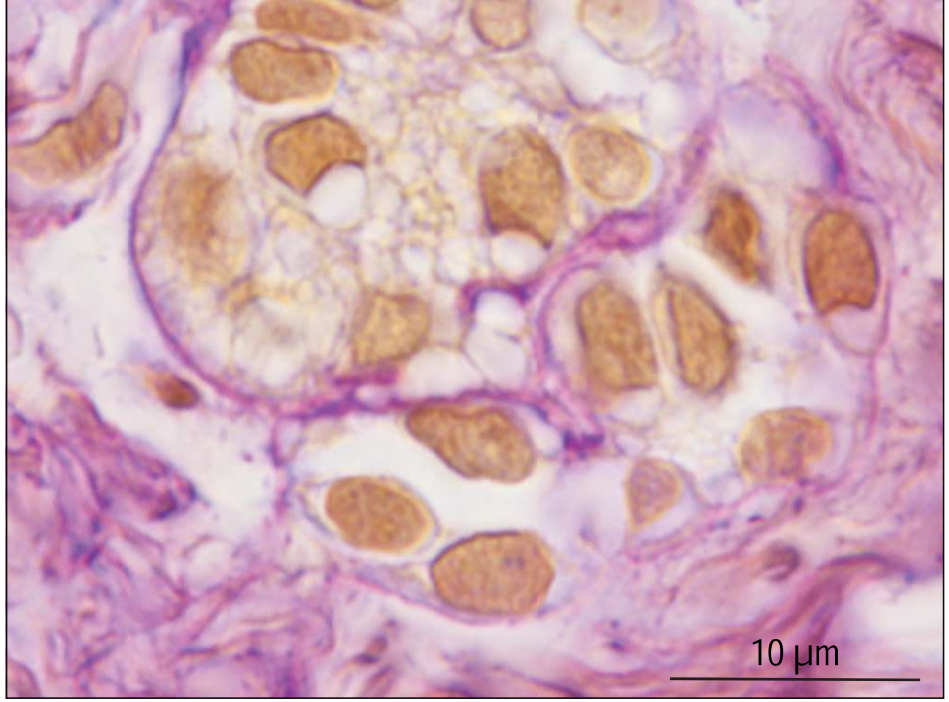

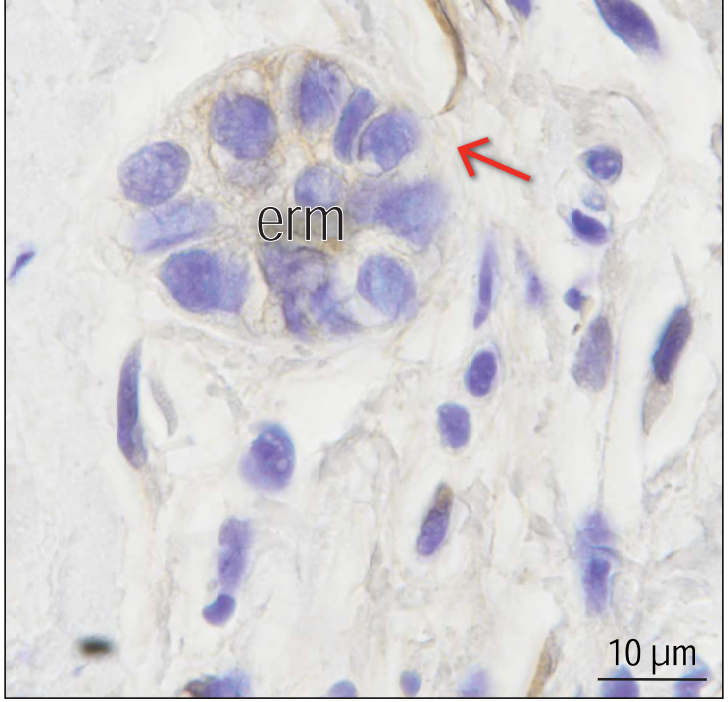

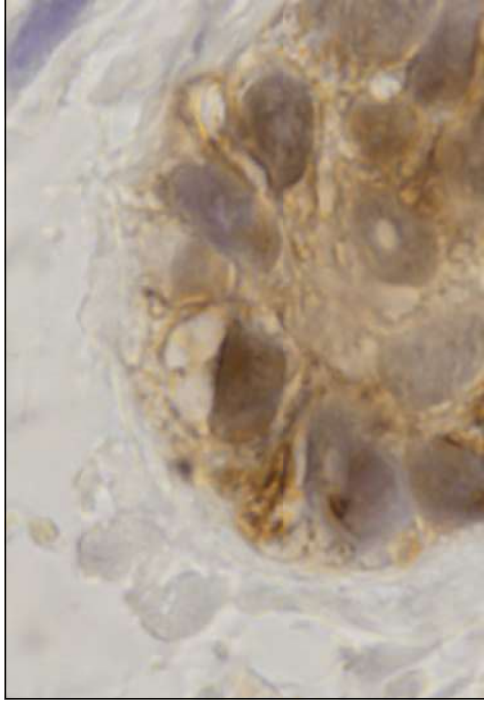

alan fibers

β III tubulin

Matrix metalloprote

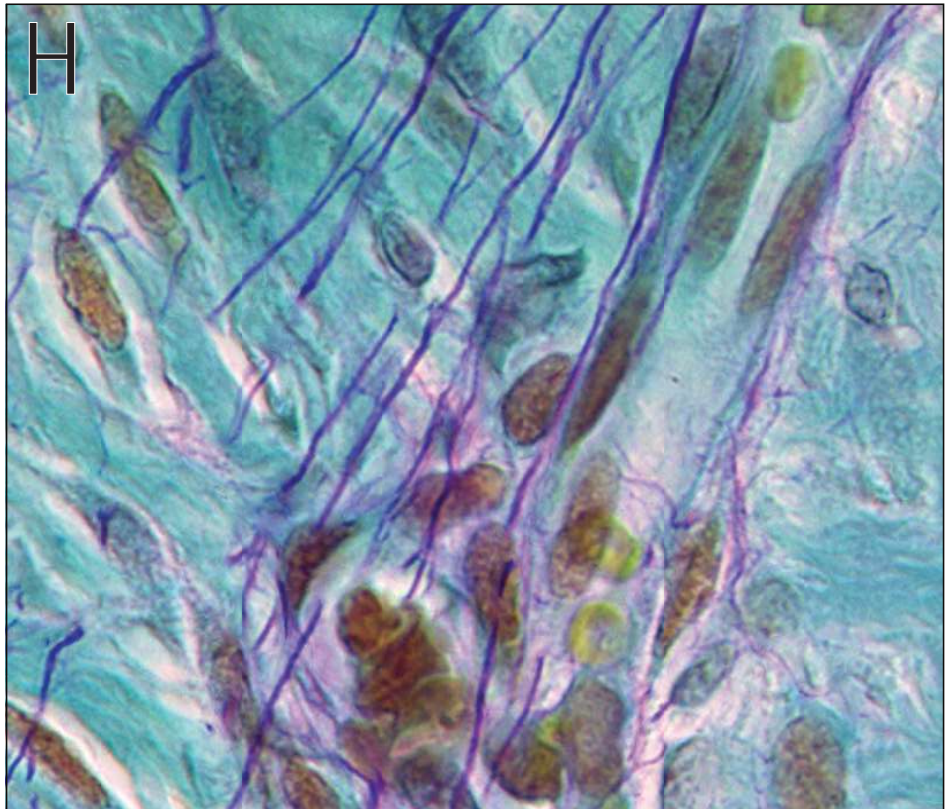

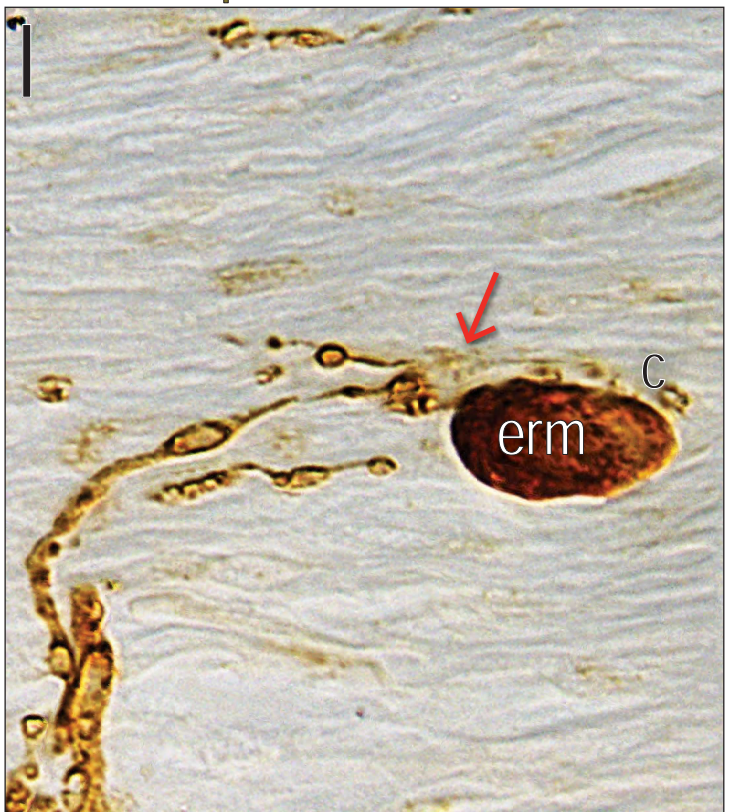

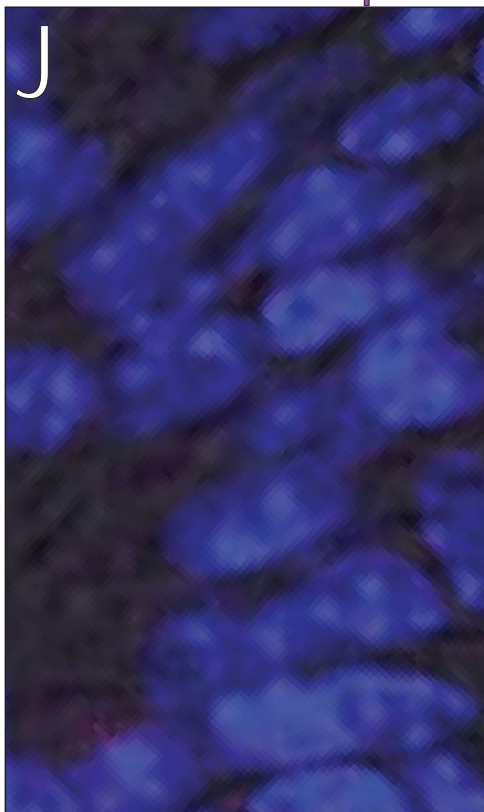

10 µm
J
d
c
10 µm
YAP
M
d
c
10 µm
β4 integrin
P
JE
50 µm
JE changes
S
oracrestal changes
0 µm
C″
c
25 µm
5 µm
D″